Строительные материалы и изделия
Construction Materials and Products

journal homepage: https://bstu-journals.ru

ISSN
2618-7183

DOI: 10.58224/2618-7183-2026-9-4-4

Mathematical modeling of heat transfer through building envelopes with cracks

Zubarev K.P. * [1, 2, 3], Dobshits V.L. [1], Kazunin V.V. [1], Sapronova Y.A. [2], Fedoseev V.D. [2], Kalinina O.V. [4]

[1] RUDN University, Russia,
[2] National Research Moscow State University of Civil Engineering, Russia,
[3] Research Institute of Building Physics of Russian Academy of Architecture and Construction Science, Russia,
[4] Enright Project Construction Limited Liability Company, Russia

Abstract. Cracks formed in building walls are frequently restored by injecting specially formulated repair grouts into the damaged areas. This study examines the effect of such repaired cracks on the thermal performance of building envelopes. Heat transfer within cracked wall sections was modeled by solving the two-dimensional steady-state heat conduction equation. Convective boundary conditions of the third kind were specified on the exterior surfaces to account for heat exchange between the wall and the surrounding environment. The truncated edges of the computational domain were assigned insulated (second-kind) boundary conditions, corresponding to zero normal heat flux. At the interfaces between adjacent materials, continuity of both temperature and heat flux was enforced through fourth-kind boundary conditions. The numerical analysis was carried out using the finite element method implemented in ANSYS Workbench 2024. Based on the obtained numerical results, a procedure was developed for constructing nomograms that characterize the specific heat losses associated with wall cracks repaired by injection grouting. The temperature fields of aerated concrete, clay brick, and reinforced concrete wall assemblies were investigated. The results indicate that injecting a repair grout into a crack increases the heat flux through the examined section in brick and aerated concrete walls, whereas the opposite effect is observed for reinforced concrete walls, where the heat flux decreases after crack injection. The simulations demonstrated that replacing the air-filled crack with injection grout increases the heat flux across the repaired region of the wall. Graphical nomograms were therefore established to estimate the heat flow through repaired cracks directly from two governing parameters – the crack depth and the crack opening width – without the need for a complete numerical solution of the temperature field. In addition, the paper presents a practical algorithm describing the application of these nomograms in engineering calculations. The developed graphical tools can be employed to evaluate the overall thermal resistance of building envelopes during reconstruction, rehabilitation, and major renovation of existing buildings.

Keywords: heat transfer, specific heat loss, cracks, injection grout, mathematical model, thermal conductivity, foam concrete, brick, reinforced concrete

*Corresponding author E-mail: zubarevkirill93@mail.ru

Received April 16, 2026; Received in revised form June 17, 2026; Accepted August 1, 2026

Please cite this article as:. Zubarev K.P., Dobshits V.L., Kazunin V.V., Sapronova Y.A., Fedoseev V.D., Kalinina O.V. Mathematical modeling of heat transfer through building envelopes with cracks Construction Materials and Products. 2026. 9 (4). 4. DOI: 10.58224/2618-7183-2026-9-4-4

1. INTRODUCTION

1.1. Cracks in Building Envelopes

Throughout the service life of a building, structural elements are inevitably subjected to crack formation. Such defects may appear in building envelopes constructed from various materials, including brick masonry, aerated concrete, foam concrete, reinforced concrete, and other widely used structural materials.

Representative examples of cracks identified in walls composed of different construction materials are presented in Fig. 1.

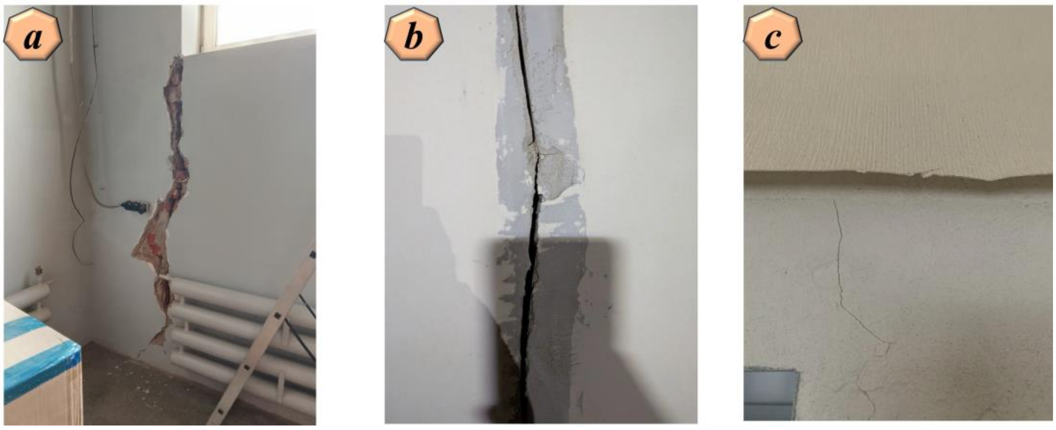

Fig. 1. Typical cracks observed in building walls constructed from different materials: (a) brick masonry; (b) reinforced concrete; (c) foam concrete.

During reconstruction and major renovation, these defects are commonly repaired by pressure injection of specially formulated repair grouts through injection packers.

Examples of repaired cracks with installed injection packers are illustrated in Fig. 2.

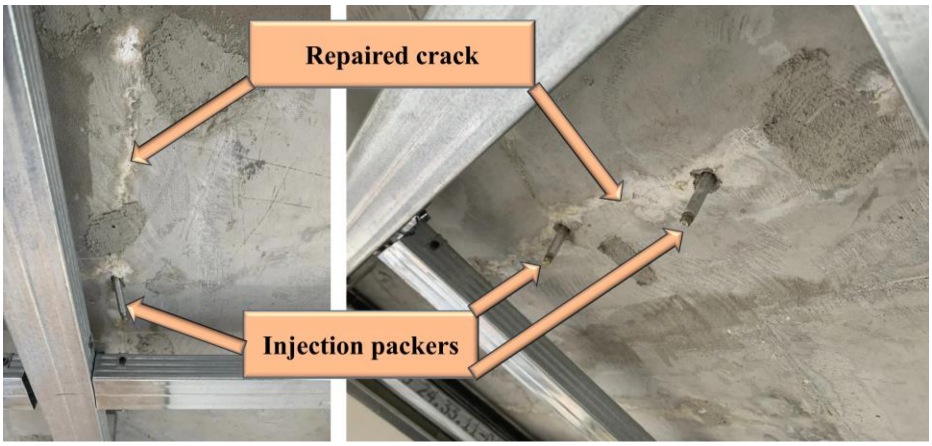

Fig. 2. Photographs of repaired cracks with installed injection packers.

1.2. Previous Studies on Crack Injection in Building Envelopes

Extensive research has been devoted to the development of materials, techniques, and technologies for repairing cracks in building structures and construction materials [1–11].

Wu et al. employed unmanned aerial vehicles integrated with oblique photogrammetry to inspect a historic masonry wall. By reconstructing a three-dimensional digital model of the structure, the authors identified 43 cracks exceeding 0.3 m in length together with 15 delaminated areas larger than 0.03 m^2 [2].

Dong et al. introduced an enhanced lightweight deep-learning model, YOLOv8-CD, for automated crack detection on concrete surfaces. According to their results, the proposed algorithm achieved higher detection accuracy while reducing computational requirements, improving processing speed, and maintaining efficient performance on mobile platforms compared with existing methods [3].

Using a Monte Carlo simulation framework, Wang et al. examined the stochastic development of crack networks in concrete. The cracked material was represented by a simplified pore-crack model, which enabled the interaction between cement slurry and damaged concrete to be investigated in detail [4].

Tselios et al. studied the performance of chemical anchors installed in solid clay brick masonry. Particular attention was given to the failure mechanisms associated with anchors embedded in both intact masonry and substrates containing pre-existing cracks [5].

Oladiran et al. evaluated the properties of epoxy-repaired concrete by comparing its performance with that of conventional concrete. Their experimental findings demonstrated that epoxy injection effectively restores the integrity of cracked concrete and may even enhance its mechanical characteristics beyond those of the original material [6].

Starczyk-Kołbyk et al. developed an environmentally sustainable rapid-hardening concrete intended for emergency repair operations and accelerated post-disaster reconstruction. The proposed material consists of low-emission multicomponent cement, crushed granite aggregate, soda–lime glass waste, aqueous sodium silicate, glass dust, and finely ground glass powder. Experimental investigations revealed that the mixture containing 5% glass aggregate exhibited the most favorable mechanical performance after 28 days of curing. The authors concluded that this material represents a promising solution for rapid repair and structural rehabilitation applications [7].

Sun et al. investigated an epoxy-based concrete specifically designed for the rapid rehabilitation of short-span and medium-span bridges. In addition to developing the concrete mixture, the authors proposed a constitutive model that describes its mechanical response as a function of temperature [8].

Chuang et al. examined the properties of a cement-based injection grout composed of Portland cement, sulfoaluminate cement, and reactive ultrafine fly ash. Their experimental study demonstrated that the optimum composition for crack injection corresponded to a water-to-binder ratio of 0.40, with the binder consisting of 75% sulfoaluminate cement, 20% Portland cement, and 5% reactive ultrafine fly ash [9].

Li et al. investigated a cementitious injection grout incorporating quartz sand as a filler material. Their results confirmed that epoxy-based repair can successfully restore—and in certain cases improve—the structural performance of cracked concrete. Following repair, the compressive strength of the specimens increased, with the maximum strength recovery ratio reaching 98.41% for specimens containing cracks 0.3 mm in width [10].

Chen et al. proposed an improved repair technique for cracked clay bricks based on enzyme-induced carbonate precipitation (EICP). By introducing a centrifugal cementation process, the authors increased the flexural strength of repaired brick specimens by 22.9% compared with conventional repair procedures [11].

1.3. Influence of Building Envelope Defects on the Thermal Performance of Buildings

Thermal irregularities directly influence the thermal performance of building envelopes. Depending on the material properties and the geometry of a structural detail, they may either increase or decrease the heat flow through the envelope [12-16].

Throughout the service life of a building, the formation of cracks introduces additional thermal irregularities into the building envelope. During reconstruction or major renovation, these defects are typically repaired by pressure injection of a repair grout. Replacing the air-filled crack with an injected material changes the heat transfer characteristics of the repaired wall section.

Cracks in external walls can significantly impair the thermal insulation performance of building envelopes. Their effect is twofold. First, the thermal resistance decreases because a portion of the wall material is replaced by air occupying the crack. Second, through-cracks may allow uncontrolled air infiltration, leading to additional heat losses.

Cracks also serve as sites for moisture accumulation. Under freezing conditions, the retained moisture accelerates the deterioration of the surrounding material. In addition, through-cracks create local thermal bridges. Numerical analyses of temperature fields have shown that the presence of cracks can reduce the thermal resistance of a wall severalfold, causing it to fall below the minimum values required by building codes. Installing thermal insulation without repairing existing cracks beforehand may shift the condensation zone toward the inner part of the wall, thereby increasing the likelihood of finishing-layer debonding and subsequent deterioration. Moisture retained within the insulation freezes at subzero temperatures, damaging its fibrous structure and impairing its insulating properties. Consequently, moisture-saturated insulation exhibits substantially lower thermal efficiency.

A variety of methods have been proposed to account for thermal irregularities in building envelopes [17-20]. Throughout much of the twentieth century, engineering calculations were commonly based on the thermal homogeneity coefficient, which provided an estimate of the reduction in the overall thermal resistance caused by structural details. However, this coefficient offered only an approximate evaluation. Today, the thermal behaviour of complex building components is generally assessed by numerical simulation of temperature fields using specialized computational software [21-24].

A comprehensive study of the influence of building-envelope defects on energy performance was reported by Rusanov et al. The authors showed that ventilated facade systems are especially sensitive to disruptions in air circulation within the ventilation cavity. When the cavity width decreases below 20 mm or becomes completely obstructed, its thermal resistance is reduced considerably. Statistical processing of infrared thermography data indicated that more than half of the inspected facades contained defects, with the majority located near window-to-wall junctions. Laboratory experiments carried out in a climatic chamber confirmed that, depending on the defect type, the thermal resistance may decrease by up to two times, while insulation debonding was identified as the most critical defect. The authors also developed mathematical models describing the combined influence of multiple defects, making it possible to improve the accuracy of building energy performance assessments. Their findings demonstrated that the simultaneous occurrence of several defects produces a cumulative effect greater than the sum of their individual contributions. The proposed methodology was validated experimentally using facade specimens containing typical construction defects, including gaps between adjacent insulation boards and voids between the insulation layer and supporting brackets. Numerical simulations performed in ELCUT were in good agreement with the experimental measurements, confirming that numerical modelling can reliably predict the thermal effects of building-envelope defects without the need for extensive full-scale testing [25].

The objective of the present study is to evaluate the specific heat losses occurring in building walls containing cracks repaired by injection grouting.

This study aims to develop a nomogram for estimating specific heat loss through wall cracks following repair by injection grouting. The proposed approach enables rapid assessment of the corresponding heat flux, providing a practical tool for evaluating the thermal performance of repaired cracks.

2. METHODS AND MATERIALS

2.1. Mathematical Model of the Temperature Field for a Cracked Building Wall

The temperature field of a building wall containing a crack was described using the two-dimensional steady-state heat conduction equation:

$$\lambda(\frac{\partial^2 t}{\partial x^2} + \frac{\partial^2 t}{\partial y^2}) = 0. \tag{1}$$

where λ – the thermal conductivity, W/(m·°C); t – the temperature, °C; x and y – the spatial coordinates, m.

Schematic representation of the repaired wall section showing the computational domain and the prescribed boundary conditions is illustrated (Fig. 3).

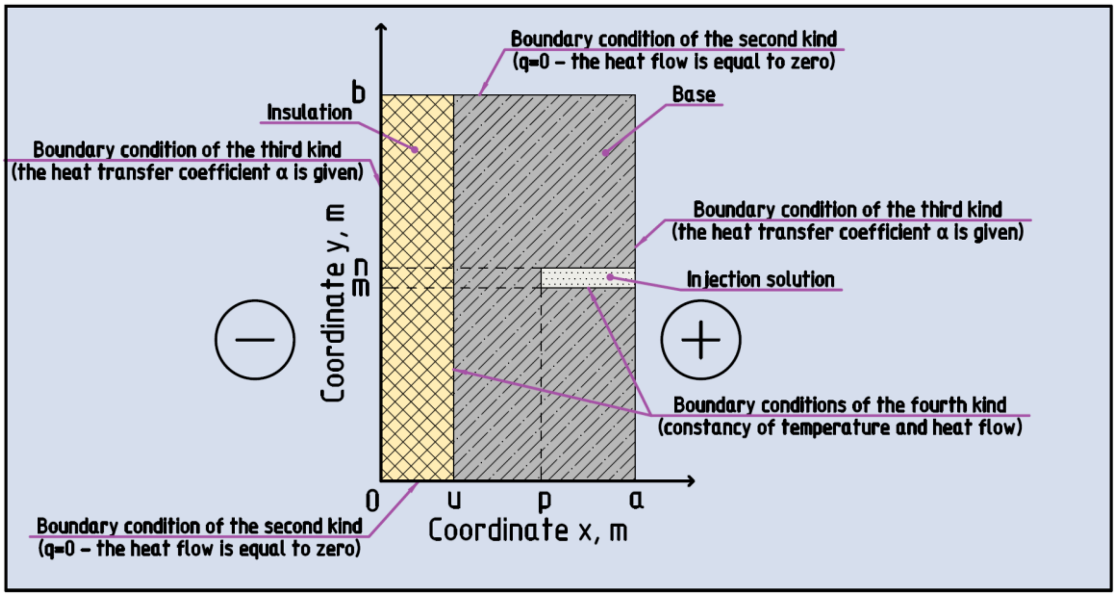

Fig. 3. Schematic representation of the repaired wall section showing the computational domain and the prescribed boundary conditions.

The computational domain Ω for the wall section under consideration is defined along the x-asix within the interval from x=0 to x=a, and from y=0 to y=b along the y-asix:

$$\Omega = \left\{x, y:\ 0 \le x \le a,\ 0 \le y \le b\right\}. \tag{2}$$

where Ω – denotes the computational domain of the analyzed wall section; a – the maximum coordinate of the domain along the x-axis, m; b – the maximum coordinate of the domain along the y-axis, m.

Robin (third-kind) boundary conditions were specified at the left and right boundaries of the wall section:

$$-\lambda \left.\frac{\partial t}{\partial x}\right|_{x=0} = \alpha_{ext}\left(t_{ext} - t_{ext.surf}\right). \tag{3}$$

$$\lambda \left.\frac{\partial t}{\partial x}\right|_{x=a} = \alpha_{in}\left(t_{in} - t_{in.surf}\right). \tag{4}$$

where α_{ext} – the external surface heat transfer coefficient, W/(m^2·°C); α_{in} – the external surface thermal resistance, (m^2·°C)/W; $t_{ext.surf}$ – the temperature of the external wall surface, °C; $t_{in.surf}$ – the temperature of the internal wall surface, °C;

Neumann (second-kind) boundary conditions were imposed on the upper and lower boundaries of the computational domain, representing thermally insulated boundaries with zero heat flux:

$$\lambda \left.\frac{\partial t}{\partial y}\right|_{y=0} = 0. \quad (5)$$

$$\lambda \left.\frac{\partial t}{\partial y}\right|_{y=b} = 0. \quad (6)$$

At the interface between the insulation layer and the structural wall material, continuity conditions were imposed in the following form:

$$-\lambda \left.\frac{\partial t}{\partial x}\right|_{x=u-0} = -\lambda \left.\frac{\partial t}{\partial x}\right|_{x=u+0}. \quad (7)$$

Similarly, the interface between the wall material and the injection grout satisfies the following continuity condition:

$$\begin{cases} -\lambda \left.\frac{\partial t}{\partial x}\right|_{x=p-0} = -\lambda \left.\frac{\partial t}{\partial x}\right|_{x=p+0} & - \text{ if } m \le y \le n \\ -\lambda \left.\frac{\partial t}{\partial y}\right|_{y=m-0} = -\lambda \left.\frac{\partial t}{\partial y}\right|_{y=m+0} & - \text{ if } p \le x \le a \\ -\lambda \left.\frac{\partial t}{\partial y}\right|_{y=n-0} = -\lambda \left.\frac{\partial t}{\partial y}\right|_{y=n+0} & - \text{ if } p \le x \le a \end{cases}. \quad (8)$$

The governing heat conduction equation was solved using the finite element method (FEM). Numerical simulations were performed in ANSYS Workbench 2024.

2.2. Algorithm for Constructing the Nomogram of Specific Heat Loss Through Injection-Repaired Wall Cracks

1. A geometric model of the builing wall is first created.
2. The temperature field is then obtained for the selected wall.
3. A crack is introduced into the geometric model of the wall.
4. The temperature field of the wall containing the crack is calculated for the selected wall node.
5. The specific heat loss through the crack filled with the injection grout is determined using the following equation:

$$\psi = \frac{q^L_{\text{with cracks}} - q^L_{\text{without cracks}}}{\Delta t}. \quad (9)$$

where ψ – the specific heat loss through the building wall filled with injection gtout, W/(m·°C); $q^L_{\text{with cracks}}$ – the linear heat flow densitypassing through the calculated wall fragment with a crack filled with injection grout, W/m; $q^{L}_{\text{without cracks}}$ – the linear heat flow density passing through the calculated wall fragment without a crack, W/m; Δt – the temperature difference between both sides of the considered building wall fragment, °C.

6. The depth and opening width of the crack are changed, and the temperature fields are recalculated. The specific heat losses are then determined using Equation (9).

7. The calculation results are presented as a nomogram of specific heat losses through the building wall with a crack filled with injection grout.

3. RESULTS AND DISCUSSION

3.1. Mathematical Modeling of a Building Wall Crack for Constructing a Nomogram of Specific Heat Losses

The results of mathematical modeling of the temperature field of building walls made of foam concrete with a thickness of 0.2 m are presented. The walls contain a through crack filled with injection grout. The crack opening width was 10 mm. Two cases were considered: a wall without insulation (Fig. 4) and a wall with insulation (Fig. 5).

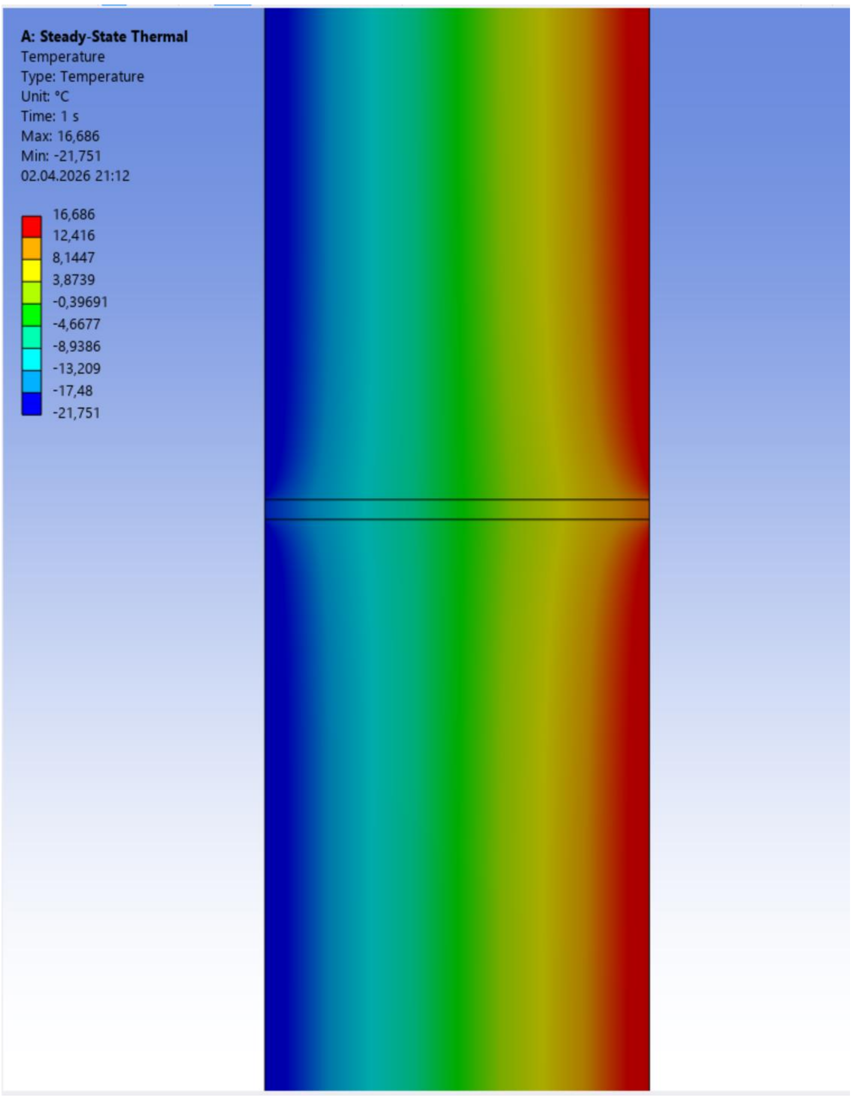

Fig. 4. Results of mathematical modeling of the temperature field of 0.2 m thick foam concrete single-layer building wall without insulation with a through crack filled with injection grout and a crack opening width of 10 mm.

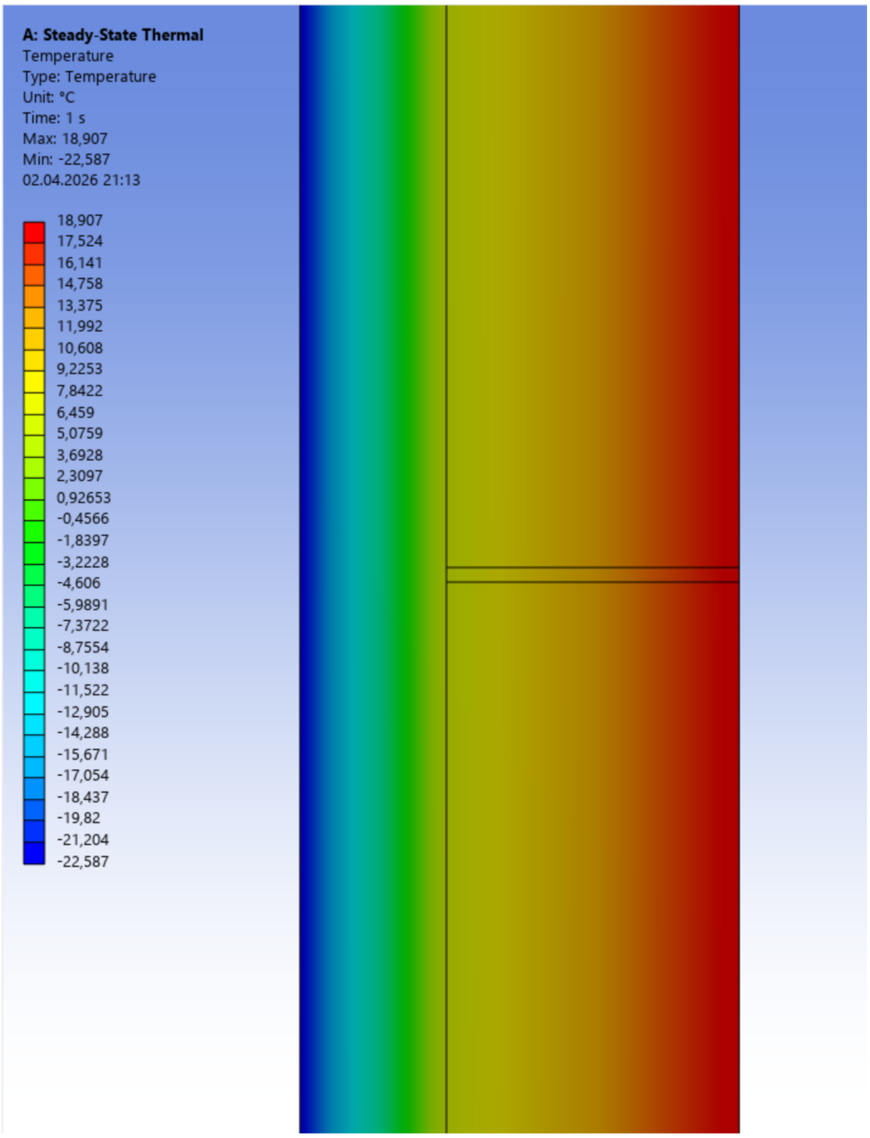

Fig. 5. Results of mathematical modeling of the temperature field of 0.2 m thick building wall insulated with 0.1 m mineral wool with a through crack filled with injection grout and a crack opening width of 10 mm.

According to the results shown in Fig. 4 and Fig. 5, the injection grout affects the temperature field distribution and causes its distortion.

As can be seen in Fig. 4 and Fig. 5, the repair zone significantly affects the local pattern of isotherms. The largest deviations occur near the inner and outer wall surfaces, where the temperature gradients become more pronounced. Owing to its higher thermal conductivity relative to foam concrete, the hardened injection grout forms a localized thermal bridge, thereby increasing heat transfer across the repaired section.

To quantify the effect of the injection grout on the linear heat flux density, the corresponding values were obtained from the numerical model for two cases. The first case represented an intact wall without a crack $q^{L}_{\text{without cracks}}$, whereas the second considered a wall containing a crack repaired by injection grouting $q^{L}_{\text{with cracks}}$. Comparison of these results made it possible to evaluate the contribution of the repair material to the heat transfer through the wall.

Linear heat flux density for a 0.2 m thick foam-concrete block wall is presented (Table 1).

Table 1. Linear heat flux density for a 0.2 m thick foam-concrete block wall is presented.

Building envelope	Linear heat flux density for the wall without a crack, W/m	Linear heat flux density for the wall with an injection-repaired crack, W/m	Specific heat loss through the injection-repaired crack, W/(m·°C)
Single-layer 0.2 m thick foam-concrete wall without thermal insulation	28.83	32.87	0.094
0.2 m thick foam-concrete wall insulated with 0.1 m mineral wool boards	10.77	11.37	0.014

Fig. 6 compares the specific heat loss associated with an injection-repaired through-crack having an opening width of 0.01 m in insulated and uninsulated foam-concrete walls 0.2 m thick.

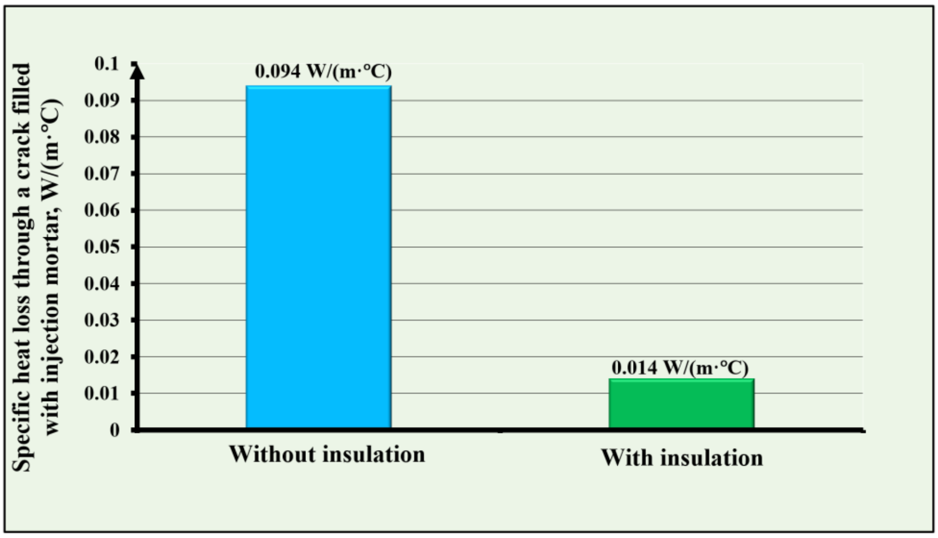

Fig. 6. Comparison of the specific heat loss through an injection-repaired through-crack (crack opening width = 0.01 m) in insulated and uninsulated 0.2 m thick foam-concrete walls.

For the uninsulated wall, the specific heat loss is 6.71 times higher than that of the corresponding wall protected by a mineral wool insulation layer.

The calculated values of the linear heat flux density for a 0.38 m thick clay brick masonry wall are summarized in Table 2.

Table 2. Linear heat flux density for a 0.38 m thick clay brick masonry wall.

Building envelope	Linear heat flux density for the wall without a crack, W/m	Linear heat flux density for the wall with an injection-repaired crack, W/m	Specific heat loss through the injection-repaired crack, W/(m·°C)
Single-layer 0.38 m thick clay brick masonry wall	68.52	70.67	0.05

Continuation of Table 2

0.38 m thick clay brick masonry wall insulated with a 0.1 m mineral wool layer	13.75	13.97	0.005

Fig. 7 compares the specific heat loss associated with an injection-repaired through-crack having a 10 mm opening in insulated and uninsulated 0.38 m thick clay brick masonry walls.

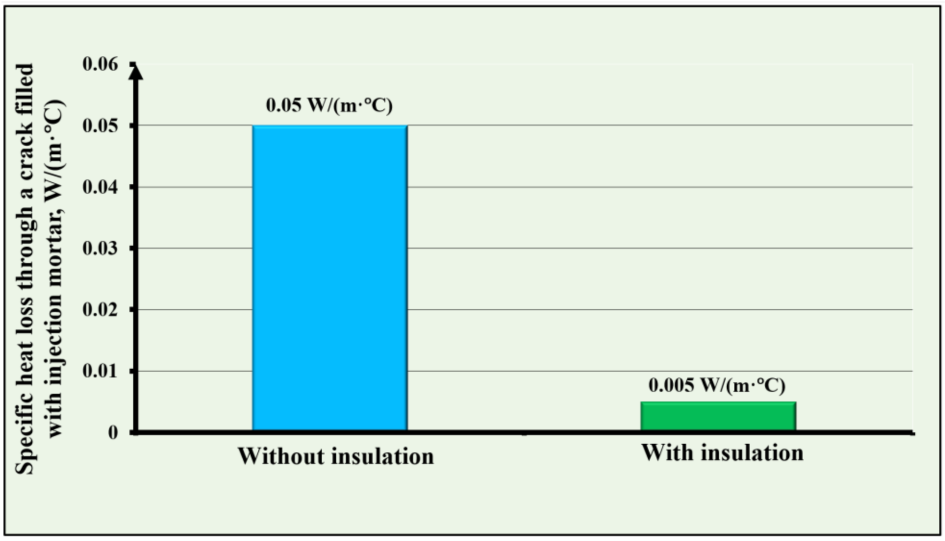

Fig. 7. Comparison of the specific heat loss through an injection-repaired through-crack with a 10 mm opening in insulated and uninsulated 0.38 m thick clay brick masonry walls.

For the uninsulated brick wall, the specific heat loss through the repaired crack is approximately ten times greater than that for the corresponding insulated wall.

Table 3 presents the linear heat flux density obtained for a 0.3 m thick reinforced concrete wall in two configurations: an intact wall and a wall containing a through-crack repaired by injection grouting with a crack opening of 10 mm. The corresponding specific heat loss through the repaired crack is also reported.

Fig. 8 compares the specific heat loss through an injection-repaired through-crack with a 10 mm opening for insulated and uninsulated 0.3 m thick reinforced concrete walls.

For the uninsulated reinforced concrete wall, the specific heat loss through the repaired crack is approximately twenty times greater than that of the corresponding insulated wall.

The comparison highlights the substantially smaller influence of the repaired crack in the insulated wall.

Table 3. Linear heat flux density for a 0.3 m thick reinforced concrete wall.

Building envelope	Linear heat flux density for the wall without a crack, W/m	Linear heat flux density for the wall with an injection-repaired crack, W/m	Specific heat loss through the injection-repaired crack, W/(m·°C)
Single-layer 0.3 m thick reinforced concrete wall	140.76	139.04	-0.04

Continuation of Table 3

0.3 m thick reinforced concrete wall insulated with a 0.1 m mineral wool layer	15.33	15.24	-0.002

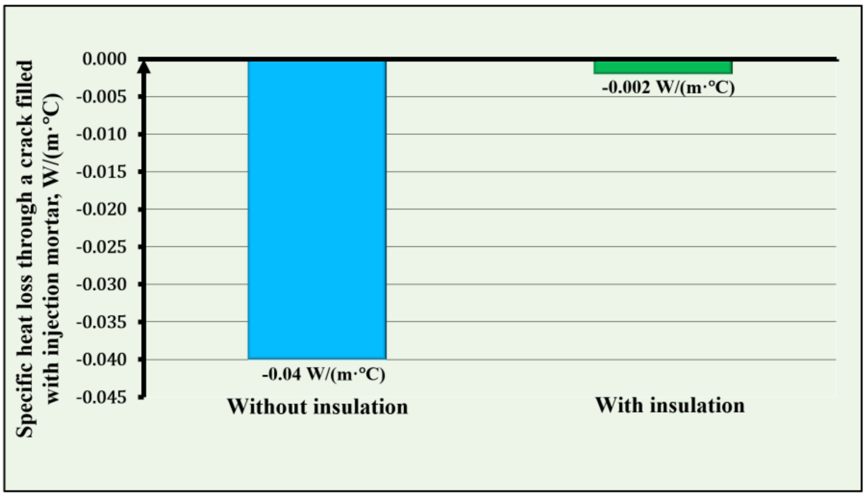

Fig. 8. Comparison of the specific heat loss through an injection-repaired through-crack with a 10 mm opening in insulated and uninsulated 0.3 m thick reinforced concrete walls.

The insulation layer lowers the overall heat flow through the building envelope, thereby reducing the contribution of the repaired defect to the wall's thermal losses.

The numerical results were subsequently used to construct nomograms for estimating the specific heat loss caused by injection-repaired cracks in building walls.

Fig. 9 shows the nomogram obtained for a 0.2 m thick foam-concrete wall. For the uninsulated wall, the specific heat loss rises steadily as both the crack depth and the crack opening increase. The highest value corresponds to a through-crack with an opening width of 0.01 m. Fig. 10 presents the corresponding nomogram for a 0.2 m thick foam-concrete wall incorporating a 0.1 m mineral wool insulation layer. The insulated wall exhibits the same overall tendency. Increasing either the crack depth or the crack opening leads to greater specific heat loss through the repaired region, while the maximum value is again associated with a through-crack having a 0.01 m opening. Fig. 11 presents the nomogram developed for estimating the specific heat loss through injection-repaired cracks in a 0.38 m thick clay brick masonry wall, whereas Fig. 12 shows the corresponding nomogram for the same wall insulated with a 0.1 m mineral wool layer. Fig. 13 shows the nomogram developed for estimating the specific heat loss through an injection-repaired crack in a 0.3 m thick reinforced concrete wall. Fig. 14 shows the corresponding nomogram for the same wall insulated with a 0.1 m mineral wool layer.

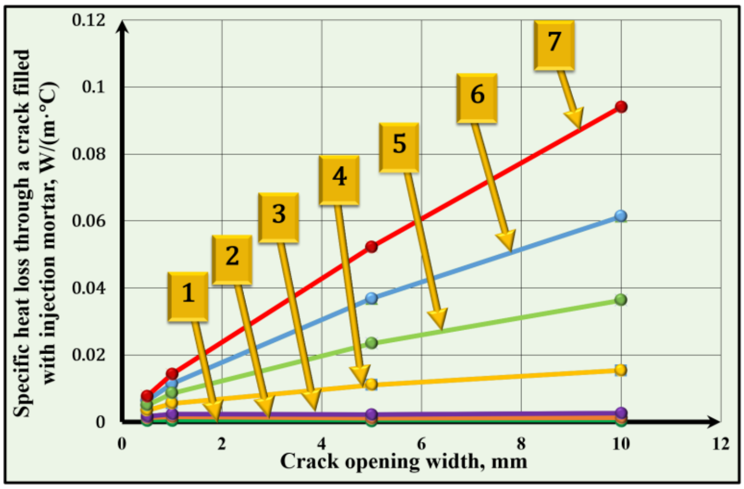

Fig. 9. Nomogram for estimating the specific heat loss through an injection-repaired crack in a 0.2 m thick foam-concrete wall (crack depth: 1 – 1 mm; 2 – 5 mm; 3 – 10 mm; 4 – 50 mm; 5 – 100 mm; 6 – 150 mm; 7 – 200 mm).

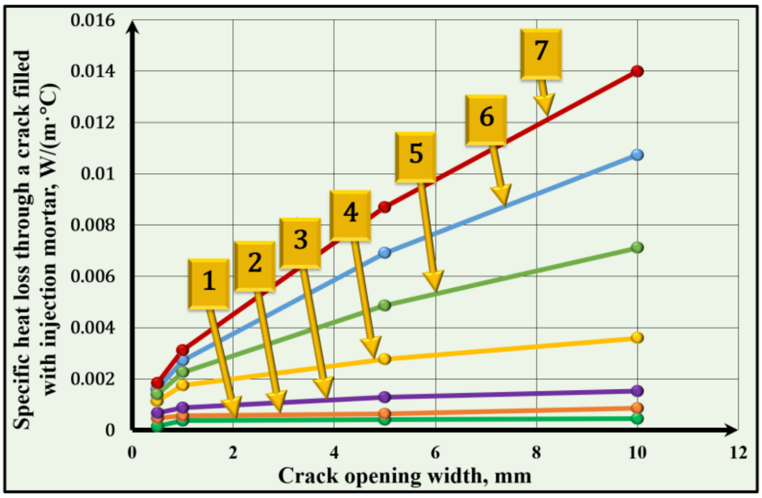

Fig. 10. Nomogram for estimating the specific heat loss through an injection-repaired crack in a 0.2 m thick foam-concrete wall insulated with a 0.1 m mineral wool layer (crack depth: 1 – 1 mm; 2 – 5 mm; 3 – 10 mm; 4 – 50 mm; 5 – 100 mm; 6 – 150 mm; 7 – 200 mm).

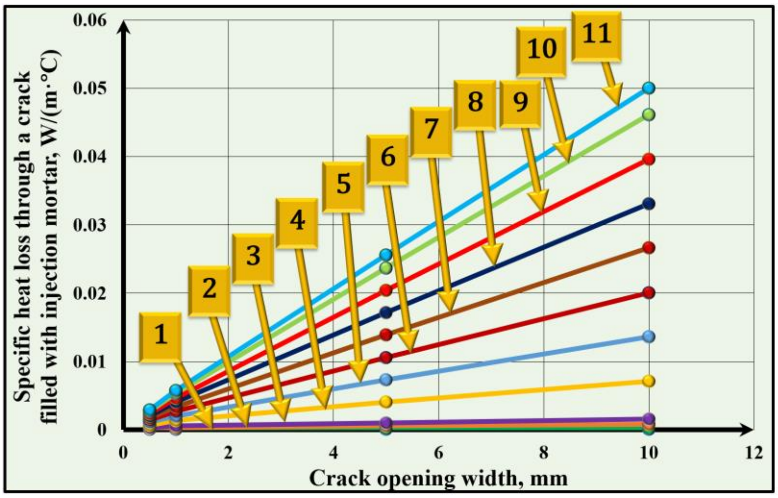

Fig. 11. Nomogram for estimating the specific heat loss through an injection-repaired crack in a 0.38 m thick clay brick masonry wall (crack depth: 1 – 1 mm; 2 – 5 mm; 3 – 10 mm; 4 – 50 mm; 5 – 100 mm; 6 – 150 mm; 7 – 200 mm; 8 – 250 mm; 9 – 300 mm; 10 – 350 мм; 11 – 380 mm).

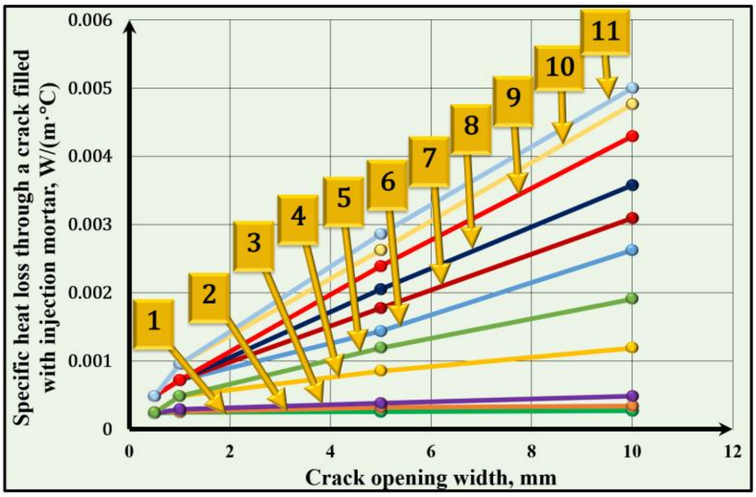

Fig. 12. Nomogram for estimating the specific heat loss through an injection-repaired crack in a 0.38 m thick clay brick masonry wall insulated with a 0.1 m mineral wool layer (crack depth: 1 – 1 mm; 2 – 5 mm; 3 – 10 mm; 4 – 50 mm; 5 – 100 mm; 6 – 150 mm; 7 – 200 mm; 8 – 250 mm; 9 – 300 mm; 10 – 350 мм; 11 – 380 mm).

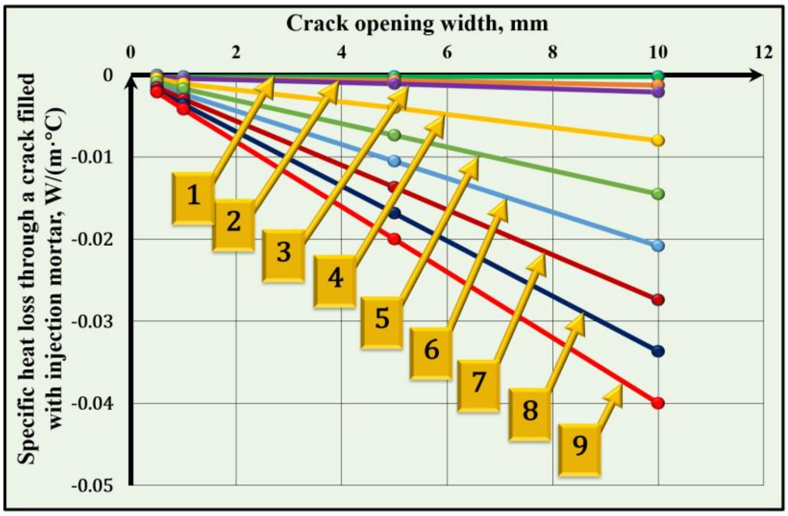

Fig. 13. Nomogram for estimating the specific heat loss through an injection-repaired crack in a 0.3 m thick reinforced concrete wall (crack depth: 1 – 1 mm; 2 – 5 mm; 3 – 10 mm; 4 – 50 mm; 5 – 100 mm; 6 – 150 mm; 7 – 200 mm; 8 – 250 mm; 9 – 300 mm).

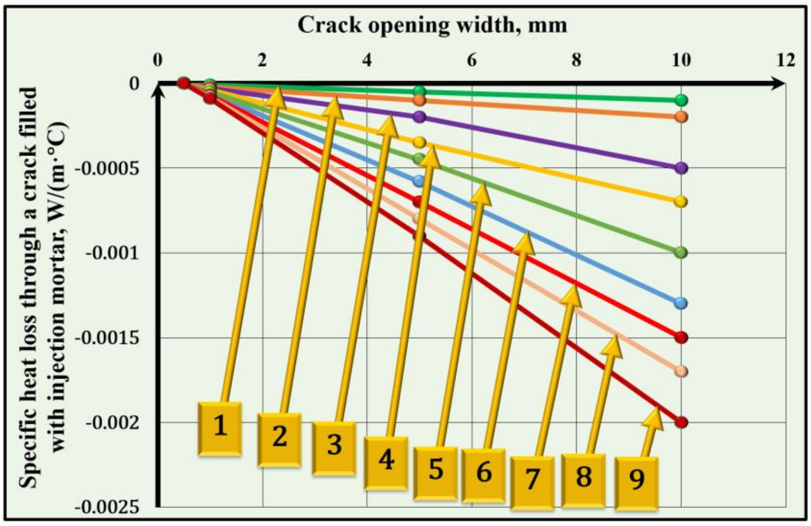

Fig. 14. Nomogram for estimating the specific heat loss through an injection-repaired crack in a 0.3 m thick reinforced concrete wall insulated with a 0.1 m mineral wool layer (crack depth: 1 – 1 mm; 2 – 5 mm; 3 – 10 mm; 4 – 50 mm; 5 – 100 mm; 6 – 150 mm; 7 – 200 mm; 8 – 250 mm; 9 – 300 mm).

3.2. Algorithm for Using the Proposed Nomograms of Specific Heat Loss Through Wall Cracks

The proposed nomograms should be applied according to the following procedure.

1. Measure the crack depth and crack opening width.
2. Locate the measured crack opening width on the horizontal axis of the nomogram.
3. Draw a vertical line from this point until it intersects the curve corresponding to the measured crack depth.
4. From the intersection point, draw a horizontal line to the vertical axis.
5. Read the specific heat loss through the repaired crack directly from the vertical axis.

4. CONCLUSIONS

The numerical analysis showed that filling a wall crack with injection grout changes the local temperature distribution and modifies the pattern of isotherms around the repaired area. The effect is much stronger in uninsulated walls, where the higher heat flow makes the influence of the repaired crack more significant.

The simulation results were used to construct nomograms for estimating the specific heat loss caused by repaired cracks. Once the crack opening and depth are known, the required heat-loss value can be obtained directly from the nomograms, eliminating the need for additional numerical simulations of the temperature field.

The numerical analysis indicates that filling a crack with injection grout leads to an increase in heat flux across the analysed wall section in clay brick and foam-concrete walls. In contrast, reinforced concrete walls exhibit a reduction in heat flux following crack repair by injection grouting.

An algorithm for using the nomograms of specific heat losses through building wall cracks filled with injection grout was developed. The proposed approach makes it possible to determine the specific heat loss through a crack based on the crack depth and crack opening width.

The proposed nomograms provide a convenient tool for assessing the thermal performance of building envelopes during reconstruction and major renovation. Their use is compatible with the evaluation procedures specified in SP 50.13330.2024 Thermal Protection of Buildings and SP 230.13330.2015 Building Envelopes. Characteristics of Thermal Non-Uniformities (Amendment No. 2).

The specific heat loss values obtained from the developed nomograms can be incorporated into the standard procedure for determining the overall thermal transmittance resistance of building envelopes.

5. ACKNOWLEDGEMENTS

This publication has been supported by the RUDN University Scientific Projects Grant System, project № 011413-2-000

REFERENCES

1. Zhang X., Zhang Y., Luo H., Peng B., Zhang Y., Yao J., Jedrzejko M.J. Experimental study and practical application of existing crack repair in concrete dam tunnels using MICP and EICP. Buildings. 2025. 15 (18). P. 3275.
2. Wu J., Shi Y., Wang H., Wen Y., Du Y. Surface defect detection of Nanjing city wall based on UAV oblique photogrammetry and TLS. Remote Sensing. 2023. 15 (8). P. 2089.
3. Dong X., Liu Y., Dai J. Concrete surface crack detection algorithm based on improved YOLOv8. Sensors. 2024. 24 (16). P. 5252.
4. Wang X., Li W., Shen M., Wang H. Numerical analysis of slurry–crack coupling in grouting repair process of multiple cracks in concrete material. Materials. 2025. 18 (11). P. 2472.
5. Tselios I., Vintzileou E., Karagiannaki D., Christidis K., Palieraki V., Welz G. Anchors to solid clay brick masonry in tension: behavior under monotonic and repeated loading for constant embedment depth. Applied Sciences. 2023. 13 (23). P. 12917.
6. Oladiran O.J., Oguntona O.A. Comparative assessment of the properties of normal concrete and epoxy-repaired concrete. Materials Proceedings. 2025. 27 (1). P. 1.
7. Starczyk-Kołbyk A., Łasica W., Kardaszuk E., Gregorczyk M. Eco-Friendly rapid-setting concrete incorporating waste-derived additives for post-disaster reconstruction. Materials. 2026. 19 (6). P. 1218.
8. Sun N., Shen C., Shen J., Wang Y. Mechanical properties and constitutive model of rapid-curing epoxy resin concrete under different temperature conditions. Materials. 2026. 19 (5). P. 996.
9. Chuang P.M., Yeih W.C., Huang R., Chen T.A., Chang J.J. A Study on cement-based crack injection materials using reactive ultra-fine fly ash, portland cement (Type I), and sulfoaluminate cement. Buildings. 2025. 15 (7). P. 1193.

10. Li G., Yan D., Liu J., Yang P., Zhang J. Experimental study on the crack concrete repaired via enzyme-induced calcium carbonate precipitation (EICP). Materials. 2024. 17 (13). P. 3205.
11. Chen Z., Xu X., Wei J., Guo X., Ke X. Mechanism of the EICP centrifugal cementation method for short-term brick crack rehabilitation. Buildings. 2026. 16 (6). P. 1251.
12. Adnan Y., Jaffar N., Razali H., Wooi L.K., Lim C.H. Field measurements of adaptive thermal comfort in naturally ventilated homes of Malaysia's hot–humid climate. Buildings. 2026. 16 (7). P. 1419.
13. Muhy Al Din S.S., Hafizi N., Altan H. Quantifying the relationship between mean radiant temperature and indoor air temperature across building orientations in hot and dry steppe climates. Atmosphere. 2025. 16 (10). P. 1132.
14. Takva Ç., Takva F.G., Çakıcı F.Z. Thermal analysis of the building envelope with infrared thermography and simulation in educational buildings in the cold climate region. Buildings. 2025. 15 (11). P. 1759.
15. Yang C., Misni A. Exploring comfort and efficiency: comparing vernacular and modern dwellings in rural Handan, northern China. Sustainability. 2026. 18 (3). P. 1575.
16. Hrčka R., Štompf P., Jochim S., Mikuš M.E., Iskra M. The measurement of hemp concrete thermal and moisture properties for an effective building construction proposal in region of Slovakia (central Europe). Materials. 2025. 18 (7). P. 1651.
17. Fan C., Chen J., Yu P. Feedback effects of air-conditioning anthropogenic heat on cooling energy consumption in residential buildings: a CFD–EnergyPlus co-simulation study. Buildings. 2026. 16 (8). P. 1610.
18. Ma X., Mao Z., Xuan H. Spatial performance optimization of high-altitude residential buildings based on the thermal buffer effect: a case study of new-type vernacular housing in Lhasa. Buildings. 2025. 15 (23). P. 4337.
19. Sun Y., Tana, Zhen Q., Yan C., Chasuna, Liu K. Spatiotemporal analysis of temperature distribution in semi-underground potato storage facilities in cold and arid regions of China. Sustainability. 2026. 18 (6). P. 2927.
20. Koo B.K., Jin H.S., Jeong J.-W. Deep learning-supported panoramic infrared framework for quantitative diagnosis of building envelope thermal anomalies. Buildings. 2025. 15 (24). P. 4423.
21. Iavorschi E., Milici L.D., Atănăsoae P., Ungureanu C. An experimental and numerical investigation of a passive façade and proposals for improving its energy performance. Energies. 2025. 18 (2). P. 359.
22. Jezierski W., Szczepaniak P., Leszczyński C. Optimization of thermal insulation parameters for vertical perimeters in buildings with single-layer walls. Buildings. 2025. 15 (3). P. 405.
23. Qin L., Qi J., Qi Y., Shi W. Energy consumption analysis and energy-saving renovation research on the building envelope structure of existing thermal power plants in China's hot summer and cold winter regions. Buildings. 2026. 16 (1). P. 169.
24. Zhangabay N., Oner A., Ibraimova U., Ibrahim M.N.M., Tursunkululy T., Utelbayeva A. Assessment and numerical modeling of the thermophysical efficiency of newly developed adaptive building envelopes under variable climatic impacts. Buildings. 2026. 16 (2). P. 366.
25. Rusanov A.E., Baiburin A.Kh., Baiburin D.A., Bianco V. Heat loss from defects of hinged facade systems of buildings. Magazine of Civil Engineering. 2020. 95 (3). P. 57 – 65.

INFORMATION ABOUT THE AUTHORS

Zubarev K.P., e-mail: zubarevkirill93@mail.ru, ORCID ID: https://orcid.org/0000-0002-7609-8521, SCOPUS: https://www.scopus.com/authid/detail.uri?authorId=57202815810, RUDN University, Candidate of Engineering Sciences (Ph.D.), Associate Professor of the Department of Construction Technology and Structural Materials, Leading Researcher of the Scientific Center of Engineering and Construction Technologies; National Research Moscow State University of Civil Engineering, Associate Professor of the Department of General and Applied Physics, Associate Professor of the Department of Computer Science and Applied Mathematics, Research Institute of Building Physics of Russian Academy of Architecture and Construction Sciences, Senior Researcher at the Laboratory of Building Thermal Physics

Dobshits V.L., e-mail: 89153383886@mail.ru, ORCID ID: https://orcid.org/0009-0005-9085-6308, RUDN University, PhD Student of the Department of Construction Technology and Structural Materials

Kazunin V.V., e-mail: kvv-vyacheslav@yandex.ru, ORCID ID: https://orcid.org/0009-0000-1005-0069, RUDN University, PhD Student of the Department of Construction Technology and Structural Materials

Sapronova Y.A., e-mail: ho5metown@gmail.com, ORCID ID: https://orcid.org/0009-0007-3032-0995, SCOPUS: https://www.scopus.com/authid/detail.uri?authorId=59235332000, National Research Moscow State University of Civil Engineering, Laboratory Research Assistant of the A.B. Zolotov Research and Education Center of Computer Modelling

Fedoseev V.D., e-mail: fedosseev.vs@gmail.com, ORCID ID: https://orcid.org/0009-0000-9513-8472, SCOPUS: https://www.scopus.com/authid/detail.uri?authorId=59234591700, National Research Moscow State University of Civil Engineering, Laboratory Research Assistant of the A.B. Zolotov Research and Education Center of Computer Modelling

Kalinina O.V., e-mail: Kalinina.kb@yandex.ru, ORCID ID: https://orcid.org/0009-0008-1089-1317, Enright Project Construction Limited Liability Company, Project Manager